Stability of axial flow in an annulus with a rotating inner cylinder

Richard M. Lueptow, Andreas Docter, and Kyungyoon Min
Department of Mechanical Engineering, Northwestern University, Evanston, Illinois 60208

(Received 25 February 1992; accepted 10 July 1992)

Flow between concentric cylinders with the inner cylinder rotating and an axial pressure gradient imposed in the annulus reveals a rich variety of flow regimes depending on the flow conditions. The occurrence of these flow regimes was studied experimentally by both visually and optically detecting the transition from one flow regime to another over a wide range of Taylor numbers for moderate axial Reynolds numbers. Seven flow regimes of toroidal vortices were identified, including Taylor vortices, wavy vortices, random wavy vortices, modulated wavy vortices, turbulent modulated wavy vortices, turbulent wavy vortices, and turbulent vortices. The toroidal vortices in these flow regimes look similar to the corresponding vortices when there is no axial flow, except that they translate with the axial flow at a speed slightly greater than the bulk axial velocity. Three flow regimes of helical vortices were observed at low Taylor numbers, including laminar helical vortices, stationary helical vortices, and wavy helical vortices. Depending on the flow parameters, the helical vortices had both positive and negative helix angles with respect to the bulk flow and appeared either stationary or moving downstream. Another flow regime consisting of the repeating sequential appearance of turbulent wavy vortices, turbulent helical vortices, and turbulent vortices was also observed.

I. INTRODUCTION

The superposition of circular Couette flow and pressure-driven axial flow in an annulus results in a situation where two mechanisms for instability are present. The curved streamlines of the circular Couette flow can result in a centrifugal instability, and the axial flow can result in a shear instability. The stability of the axial flow through an annulus with a rotating inner cylinder is important in several engineering applications, including journal bearings, biological separation devices, and rotating machinery.

Taylor's analysis of the stability of circular Couette flow can be extended to include an axial flow in the annulus for the transition from laminar Couette–Poiseuille to axial flow with toroidal Taylor vortices. The first such analyses were for the case of axisymmetric disturbances in a narrow annular gap,[1,2] later extended to arbitrarily wide annular gaps.[3,4] The resulting flow instability consists of toroidal Taylor vortices translating with the axial flow. When the restriction to axisymmetric disturbances is relaxed to allow asymmetric disturbances, the appearance of pairs of helical[5] vortices is predicted for axial Reynolds numbers above a transition value.[6–8] The inclination of the helical vortices is opposite that of the path of the stable circular Couette flow with an imposed axial flow. Experimental evidence confirms that the vortices are toroidal at low Reynolds numbers and become helical at higher Reynolds numbers.[7,9,10] In all cases, the axial flow stabilizes the circular Couette flow, such that transition to Taylor vortex flow occurs at a higher Taylor number than with no axial flow.[9–13] Recently, the transition from stable circular Couette flow to traveling Taylor vortex flow has been studied in an attempt to distinguish between absolute and convective instability.[14,15]

All the studies mentioned above were concerned with the first instability transition: from laminar Couette–Poiseuille flow to translating toroidal vortex flow or helical vortex flow. The earliest study of higher-order instability transitions was undertaken by Kaye and Elgar[16] and extended by others.[17,18] Kaye and Elgar varied the flow over a wide range of Taylor numbers and axial Reynolds numbers and found two flow regimes in addition to laminar Couette–Poiseuille flow and Taylor vortex flow. At high Taylor numbers they found a flow regime consisting of turbulent Taylor vortices, and at high Reynolds numbers they found fully turbulent flow with no vortices. Their results indicate that the transition from laminar nonvortical flow to vortex flow is stabilized by the axial flow, while the transition from laminar flow to turbulent flow is destabilized by the circular Couette flow.

In the absence of axial flow, several other unstable flow regimes consisting of toroidal vortices have been experimentally observed as the Taylor number is increased. These flow regimes include wavy vortex flow, modulated wavy vortex flow, and several regimes of turbulent vortex flow.[19,20] As a result of the experimental techniques that they used, the Kaye and Elgar study and its extensions did not differentiate between these different regimes known to exist for zero axial flow. However, Schwarz *et al.*[10] identified the appearance of laminar wavy vortex flow for nonzero axial flows. They found that, like the first instability, the transition from Taylor vortex flow to the wavy vortex flow is delayed to a higher Taylor number when an axial flow is imposed. Two other studies have mentioned higher-order transitions and flow regimes that are the focus of the research presented here. Kataoka *et al.*[21] present a map of the flow regimes in the Taylor number–Reynolds number plane for circular Couette flow with an imposed axial flow, although they offer a minimal explanation of their experimental methodology or their results. Bühler and Polifke[22]

 0899-8213/92/112446-10$04.00

also present a map of the flow regimes for a limited range of Taylor and Reynolds numbers. Since their emphasis is on the helical vortex flow at low Taylor numbers, they do not differentiate between nonwavy and wavy vortex flow or other higher-order instabilities. Except for these studies that briefly mention higher-order transitions, information on flow regimes for circular Couette flow with an imposed axial flow is not available.

The aim of the present work is to identify the flow regimes for circular Couette flow with an imposed axial flow in the annulus and to provide a map of the flow regimes in the Taylor number–Reynolds number plane. We identify flow regimes known to exist for circular Couette flow with no axial flow that were identified by Fenstermacher *et al.*,[19] but were not differentiated by Kaye and Elgar.[16] We also identify flow regimes not previously described. Further, we provide more detailed results than have been provided by either Kataoka *et al.*[21] or Bühler and Polifke.[22]

In the present work the axial Reynolds number is defined as $\mathrm{Re}=wd/\nu$, where w is the bulk axial velocity based on the flow rate, d is the width of the annular gap, and ν is the kinematic viscosity. The Taylor number, which relates the centrifugal forces to the viscous forces, has several different forms. We use $\mathrm{Ta}=r_i\Omega d/\nu$, where r_i is the radius of the inner cylinder and Ω is the rotational velocity of the inner cylinder. This form of the Taylor number, often called a rotating Reynolds number, is used because it is simple and consistent with the form used in several recent studies.[6,19,20] However, it omits the effect of the radius ratio, $\eta=r_i/r_o$, where r_o is the radius of the outer cylinder. Another form of the Taylor number[4] that includes the radius ratio, such as $T=\mathrm{Ta}^2[4(1-\eta)/(1+\eta)]$, may be appropriate for comparisons of data obtained at different radius ratios.

II. EXPERIMENTAL APPARATUS AND PROCEDURE

Experiments were performed using a cylinder system shown in Fig. 1. The outer cylinder is made from a 10.379 $\pm$0.011 cm i.d. (0.503 cm thick) transparent acrylic tube that permits optical access. The inner cylinder is a 8.890 $\pm$0.003 cm o.d. acrylic tube with a length of $L=30.5$ cm. The resulting radius ratio is $\eta=r_i/r_o=0.848$, and the aspect ratio is $\Gamma=L/d=41$. The inside of the inner cylinder was painted black to enhance contrast for flow visualization. The end walls of the inner cylinder are mounted on a stainless steel shaft, and the assembly was trued on a lathe to assure concentricity. The shaft turns in self-lubricating bearings in the upper and lower end caps that are fitted to the ends of the outer cylinder. The cylinders are concentric to within $\pm$0.003 cm. The inner cylinder is driven by a dc motor with tachometer feedback control coupled to the shaft above the upper end cap. The rotational speed of the motor varied by less than 0.1% over the course of an experiment.

Special care was taken to assure azimuthally uniform axial flow into the annulus using a flow distributor in the upper cap, as shown in Fig. 1. Fluid enters a deep annular groove in the upper cap tangentially through four inlet

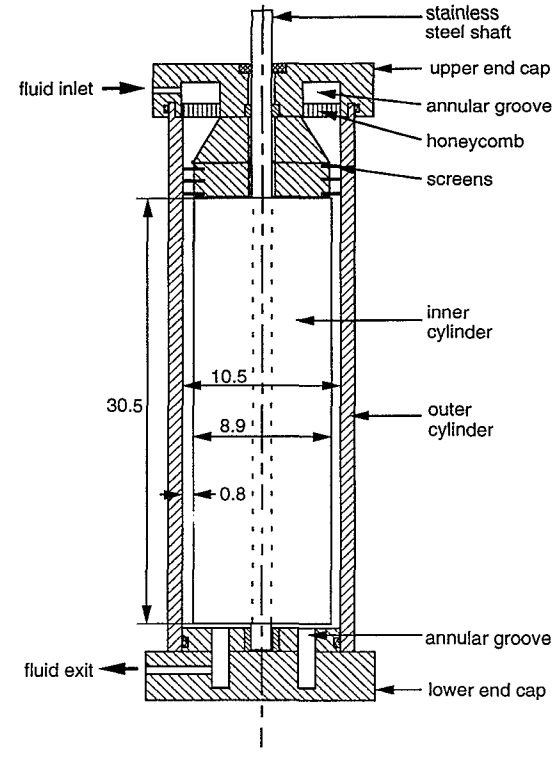

FIG. 1. Sketch of cylinder system (dimensions are in centimeters).

ports resulting in a spiral flow that uniformly distributes the fluid. An aluminum honeycomb ring with cells of 0.1 cm diam and 0.5 cm long removes the azimuthal component of velocity and directs the fluid axially. The fluid moves axially through a contraction section, finally passing through a series of three stainless steel screens with a mesh size of 0.1 cm to suppress any large eddies. The inlet ports, honeycomb flow straightener, and the screens are all fixed to the upper end cap. The flow distributor is designed so that the annular gap at the exit of the flow distributor is identical to the annular gap between the inner rotating cylinder and the outer stationary cylinder. Visualization of the flow in the test section just below the lowest screen with no inner cylinder rotation shows a circumferentially uniform axial flow. The fluid exits the annulus by flowing radially in the 2 mm gap between the lower end wall of the inner cylinder and the lower end cap. Flow visualization using a sheet of laser light in a radial plane shows that vortices reaching the end of the annulus simply slip radially inward between the inner cylinder and the lower end cap with no visible influence upstream in the annulus.

Fluid flows out of the lower end cap through an electromagnetic flow meter to a reservoir. The fluid is pumped from the reservoir to a constant head tank mounted above the cylinder system. The constant head tank supplies the fluid to the inlet ports in the upper end cap of the cylinder system. The axial flow rate is adjusted by varying both the level of the constant head tank and a valve downstream of the cylinder system.

The working fluid was a mixture of deionized water and glycerol with a typical kinematic viscosity of 0.04

cm^2/sec. Titanium dioxide coated mica particles (Superpearl 120c, Mearl Corp.) were added to the water–glycerol mixture at a mass concentration of up to 0.25% to permit flow visualization. The flakelike particles tend to align themselves with stream surfaces and act as tiny mirrors reflecting incident light to allow visualization.[23] Although problems have been noted in the use of reflective particles in a vertical Taylor–Couette system,[24] the small size of the particles (5–25 μm across and about 0.5 μm thick) and the motion of the fluid through the flow circuit prevented sedimentation of the particles during an experiment.

To mix the particles and assure a uniform temperature of the working fluid, it was circulated through the flow system for at least 30 min prior to an experiment. A sample of working fluid was filtered to remove particles and several viscosity measurements were made with a Cannon–Fenske viscometer. Based on the results of Andereck *et al.* [20] the low concentration of particles should have negligible effect on the viscosity of the working fluid. As a check of the viscosity measurement, the rotational speed at which the transition from laminar circular Couette flow to Taylor vortex flow was measured for the case of no axial flow and compared to the analytically predicted Taylor number for transition.[25,26]

Although visual observation of the flow is sometimes adequate to detect the transition of the flow from one flow state to another, often the transition is difficult to identify. For instance, the transition from wavy vortex flow to modulated wavy vortex flow is very subtle, because it is visually observed as a slight flattening of the wavy vortex outflow boundary.[27] However, spectral analysis of a time-dependent property of the flow has been successfully used to detect transitions from one flow regime to another since a frequency component appears or disappears upon transition.[19,20,27,28]

In these experiments the time-dependent property of the flow used to detect transitions was reflected light. A 15 mW He–Ne laser was used to illuminate a small region of the annulus. A photodiode (EG & G model UV-360 BG), positioned outside of the outer cylinder near the illuminated region of the annulus, sensed the light reflected from the titanium dioxide coated mica particles suspended in the working fluid. The photodiode was positioned about one-third of the cylinder height from the bottom of the inner cylinder to avoid entrance and exit effects. The exact position of the sensing photodiode with respect to the illuminated region, while not critical, was adjusted to provide a signal with the largest amplitude and clearest periodicity. The photodiode signal was low-pass filtered to remove 60 Hz noise and then offset and amplified using home built electronics to bring the signal into an acceptable range for the analog-to-digital converter (GW Instrument MacADIOS II in a Macintosh II computer). Typically 512 points were sampled at 0.0625 sec intervals, and the power spectrum of the signal was calculated with a frequency resolution of 31.25 mHz. Ten power spectra were ensemble averaged to reduce random noise that sometimes hides the frequency components of interest.

The power spectrum of the photodiode signal can indicate up to three fundamental frequencies related to the flow, along with their harmonics. The lowest frequency, f_A, results from the variation in the reflected laser light as vortices translate downstream passing the illuminated region. This frequency usually has the highest energy content. Azimuthal waviness results in a second frequency, f_1, as the waves pass the measurement location, causing a variation in the reflected light. The modulation of the waviness results is a third frequency, f_2, which is lower in frequency than that caused by the azimuthal waviness. Turbulence raises the spectral level at all frequencies due to the random reflection of light. Figure 2 shows an example of the power spectrum for wavy vortex flow indicating f_A due to vortex translation, f_1 due to azimuthal waviness, and several harmonics and frequency combinations. Although the power spectrum is helpful in identifying flow transitions, a frequency component related to the flow often gradually appears or disappears with increasing Reynolds or Taylor number. In this work, a frequency component was said to be present when it, or its harmonics, was clearly evident above the noise level of the power spectrum.

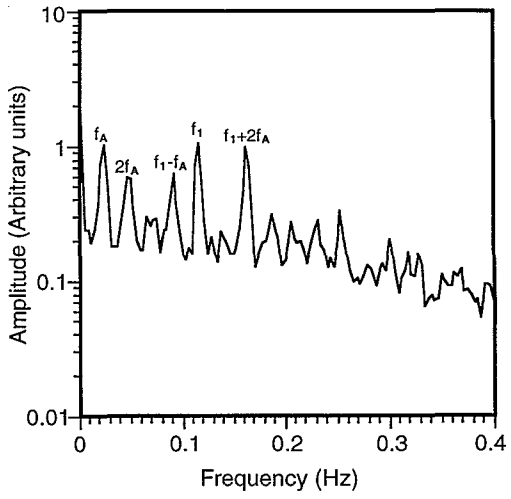

FIG. 2. Spectrum of reflected light for wavy vortex flow with an axial flow imposed showing the frequency of passage of vortices, f_A, and the frequency of the azimuthal waviness, f_1.

After circulating the fluid and measuring the kinematic viscosity, the axial flow to provide a given Reynolds number was set by adjusting the axial flow valve downstream of the cylinder with no inner cylinder rotation. An experiment began by increasing the Taylor number in increments of Δ Ta=20. Near the transition boundaries at low Taylor number, the increment was Δ Ta=2 to be assured of noting the transition with accuracy. Although the rotational speed was adjusted manually, the rate of angular acceleration was kept at less than 0.3 rad/min^2 by use of a stopwatch. The flow was allowed 5 min to reach equilibrium before recording the photodiode signal and calculating the power spectrum. Above Taylor numbers of 200, the Taylor number was increased by increments of Δ Ta=100 until turbulent Taylor vortices appeared at a Taylor number as high as 2900. Flow regimes were identified by their spectral

characteristics and confirmed by visual observation. In addition, the frequency of axial and azimuthal waves passing a fixed point on the outer cylinder was determined with a stopwatch for comparison to the power spectrum. The above procedure was repeated when the Reynolds number was increased by an increment of either 3 or 5. In this way a grid of measurement points was generated for Reynolds numbers ranging from 0 to 37 and Taylor numbers ranging from 0 to 2900.

Uncertainty in the Taylor number and the Reynolds number results from variation in fluid viscosity due to temperature changes, asymmetries in the cylinder dimensions, along with difficulties in measuring the rotational speed and the axial volume flow rate. A particular problem in this experimental apparatus is that the temperature gradient in the room results in a higher fluid temperature at the upper reservoir than at the cylinder or lower reservoir. For $Re \geqslant 9$ this is not a problem because fluid circulation results in a well-mixed fluid of uniform temperature. At $Re=0$ it is also not a problem, since the vertical temperature gradient is limited to the fluid in the cylinder and is very small. However, at $Re=3$ and $Re=6$, the axial flow is too low to promote adequate mixing to overcome the ambient temperature gradient in the room resulting in a significant error in the value of the viscosity. At these Reynolds numbers we estimate an uncertainty of 3%–4% for both the Reynolds number and the Taylor number, primarily as a consequence of the effect of temperature on the fluid viscosity. At higher Reynolds numbers and with no axial flow the uncertainty in the Taylor number is less than 2%, and the uncertainty in the Reynolds number is less than 1%.

As a check on the operation of experimental apparatus with no axial flow, the ratio of the Taylor number for higher-order transitions to the critical Taylor number for the first transition, Ta/Ta_{cr}, was compared to the results of Fenstermacher *et al.*[19] and Andereck *et al.*[20] for similar radius ratios, η. While not identical, the Taylor numbers for transition are similar, as shown in Table I. The largest deviation is for the cases of the transition to turbulent modulated wavy vortices and the transition to turbulent Taylor vortices where the present results deviate from previous results by 13%. Most likely the discrepancies in the Taylor numbers for transition are a consequence of the lack of a sharp difference in the character adjacent flow regimes, even when using power spectra of the reflected light to identify transition. Another problem is that different circumferential wave numbers for wavy vortex flow have different Taylor numbers for transition.[26] In addition, different aspect ratios, measurement techniques, and experimental setups can contribute to discrepancies. Nonetheless, the agreement between the present results and previous studies indicates that the experimental apparatus performs adequately.

III. RESULTS

The principal result of this work is the map of observed flow regimes in the Reynolds number–Taylor number plane shown in Fig. 3. The points shown on the figure indicate the Reynolds number and Taylor number at which the flow was observed for $Ta \geqslant 300$. The curves dividing one flow regime from another are sketched between the points where two different regimes were observed. While some of the transitions are sharp, most are less distinct. Thus, the curves sketched in Fig. 2 should not be construed as sharp boundaries between flow regimes, but simply as a visual guide. A map of the flow regimes for low Taylor numbers is shown in Fig. 4. The acronyms for the flow regimes are defined in Table II.

TABLE I. Comparison of Taylor numbers for transition from one flow regime to another.

	Ref. 20	Ref. 19	Present results
Radius ratio, η	0.883	0.877	0.848
Aspect ratio, Γ	30	20	41
Theoretical Ta_{cr}[a]	122	119	108
Experimentally measured Ta_{cr}	~120	Not given	108
Type of flow	Ta/Ta_{cr}	Ta/Ta_{cr}	Ta/Ta_{cr}
Taylor vortices	1.0	1.0	1.0
Wavy vortices	1.17	1.2	1.16
Modulated wavy vortices	8.2	10.1	~8.8[d]
Turbulent modulated wavy vortices[b]	11.3	~12	~12.5[d]
Turbulent wavy vortices[b]	[c]	19.3	~17.1[d]
Turbulent Taylor vortices[b]	[c]	21.9	~23.6[d]

[a]Numerical calculations based on the linear stability analysis of Refs. 25 and 26.
[b]Fenstermacher *et al.*[19] call these flows "weakly turbulent... ."
[c]Andereck *et al.*[20] do not differentiate between the different regimes of turbulent vortex flow.
[d]These values are approximate since the Ta number was incremented in steps of $\Delta Ta = 100$. For instance, modulated wavy vortex flow occurs for $900 \leqslant Ta \leqslant 1000$, so Ta/Ta_{cr} was calculated as $\frac{950}{108} = 8.8$.

At low Taylor numbers, laminar circular Couette flow superimposed with laminar axial Poiseuille flow (CP) exists in the annulus. The theoretically derived transition to Taylor vortex flow occurs at $Ta = 108$ for zero axial flow based on linear stability calculations.[25,26] The experimental results agree closely with the theory, as shown in Fig. 4. When an axial flow is present, the laminar Taylor vortices (LV) move downstream with the axial flow, but otherwise appear unaffected by the axial flow for Reynolds numbers up to about 9, as shown in Fig. 5(a). The axial wavelength of the vortex pair is $2.1d$. The entering axial flow results in a vortex-free region at the top of the annulus.

At higher Reynolds number the vortices are no longer individual toroids, but form a pair of helical vortices with an axial wavelength of $2.0d$. The vortices are denoted HV (helical vortices) in Fig. 4 and translate downstream, appearing as shown in Fig. 5(b). This vortex has a negative helix angle of 2.7° with respect to the direction of the flow, which corresponds to the expected helix angle if the vortex were shifted axially by $2d$ (one vortex pair) for each revolution. The helical vortices appear to move downstream, as a result of the combination of the barber-pole effect of rotation of the helical vortices and the translation of vortices in the downstream direction. Table III presents the Reynolds number for transition from toroidal vortices to

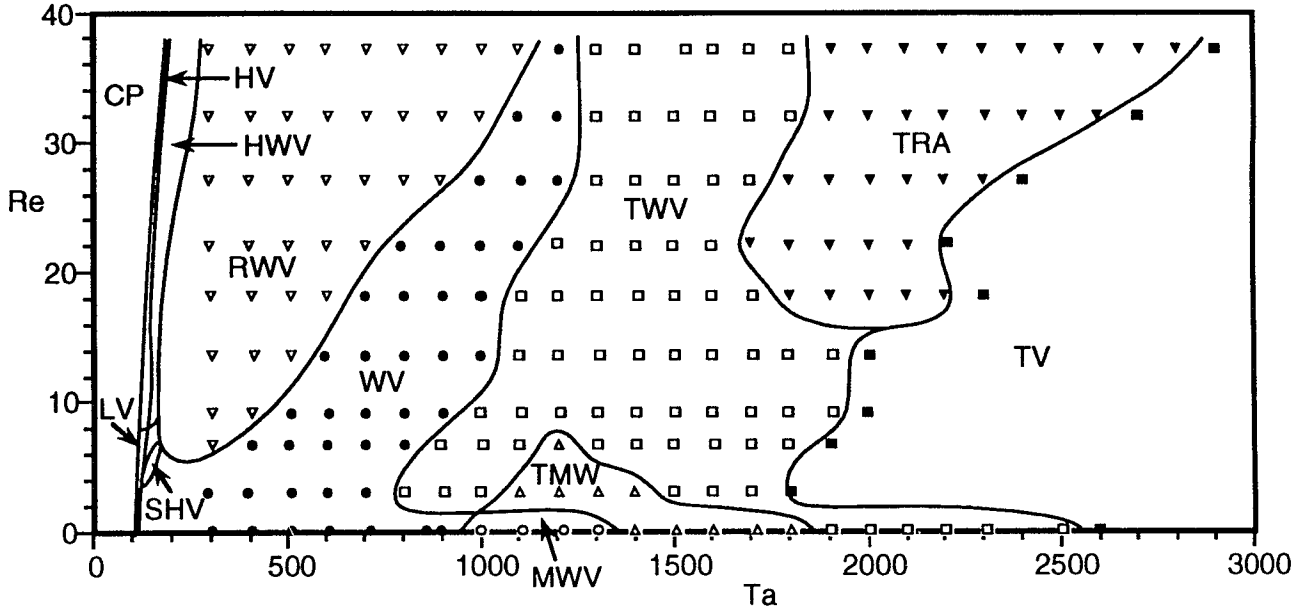

FIG. 3. Flow regimes for circular Couette flow with an imposed axial flow. Symbols represent measurement points for Ta≥300. The curves sketched between flow regimes are a visual guide, but should not be construed as sharp boundaries.

helical vortices for a variety of cases that have been studied. The transition to helical vortex flow occurs at a somewhat lower Reynolds number in the present case than in other studies. The difference may be a result of the effect of the finite aspect ratio on the flow.

The axial flow stabilizes the circular Couette flow, as predicted in earlier studies. Figure 6 compares the results for this first transition to the theoretical prediction of Chung and Astill[6] who provide results for radius ratios η of 0.5, 0.75, and 0.95. Interpolation using a spline fit to the Chung and Astill data provided the curve shown for $\eta=0.85$ for Re≥20. However, a spline fit to the data was inaccurate for Re<20 because of the nonlinearity of the dependence of the critical Taylor number on η. To avoid this problem, a straight line was drawn from the value at Re=20 to the critical Taylor number for zero axial flow. Clearly, the present data for $\eta=0.848$, as well as the experimental data for $\eta=0.5$,[7] $\eta=0.738$,[14] and $\eta=0.95$[9] match the theoretical prediction.

Taylor vortex flow becomes unstable at Ta=125 for zero axial flow, and the vortices develop an azimuthal waviness. When an axial flow is imposed, the flow is similar in appearance to wavy vortex flow with no axial flow, except that the vortices translate downward. This flow, denoted wavy vortices (WV) in Fig. 4, is shown in Fig. 7(a). These vortices are axially elongated with an axial wavelength of the vortices of 3.4*d*, substantially greater than that of other flow regimes. As the Reynolds number is increased above Re=9, the wavy vortices adopt a helical motion while retaining their waviness. These helical wavy vortices (HWV) are shown in Fig. 7(b) and move downstream with the axial flow. The waviness is difficult to observe in the photograph, although it was easily detected using the spectrum

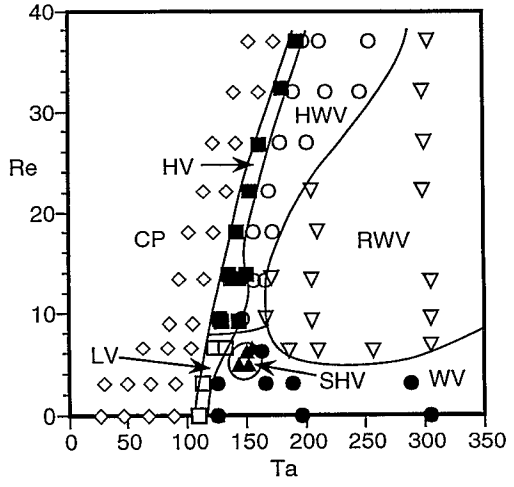

FIG. 4. Detail of flow regimes for low Taylor number. Symbols represent measurement points. The curves sketched between flow regimes are a visual guide, but should not be construed as sharp boundaries.

TABLE II. Acronyms for flow regimes.

CP	Couette–Poiseuille flow
HV	Laminar helical vortices
HWV	Laminar helical wavy vortices
LV	Laminar vortices
MWV	Laminar modulated wavy vortices
RWV	Random laminar wavy vortices
SHV	Stationary helical vortices
TMW	Turbulent modulated wavy vortices
TRA	Transitional flow
TV	Turbulent vortices
TWV	Turbulent wavy vortices
WV	Laminar wavy vortices

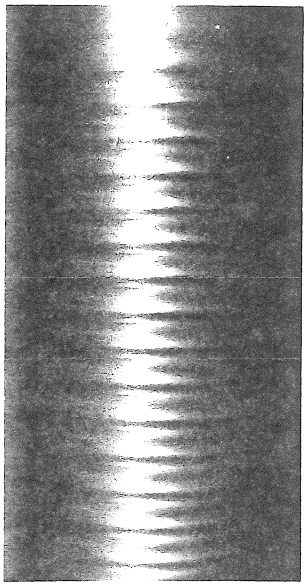

(a)

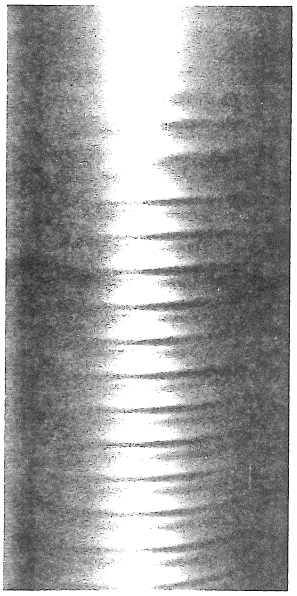

(b)

FIG. 5. (a) Flow visualization of laminar vortices (LV) for Re$\approx$7 and Ta$\approx$120. The dark regions are boundaries between vortex pairs. The inner cylinder is rotating left to right. (b) Flow visualization of laminar helical vortices (HV) for Re$\approx$10 and Ta$\approx$130.

TABLE III. Comparison of Reynolds number for transition to laminar helical vortex (HV) flow.

Radius ratio η	Re for transition to helical vortices	Type of study	Reference
0.5	24	Analytical	7
0.75	10–20	Analytical	6
0.77	10–20	Analytical	8
0.848	9	Experimental	Present study
0.95	10–20	Analytical	6
0.95	15	Experimental	10
0.95	10–20	Analytical	8
0.95	21	Experimental	9

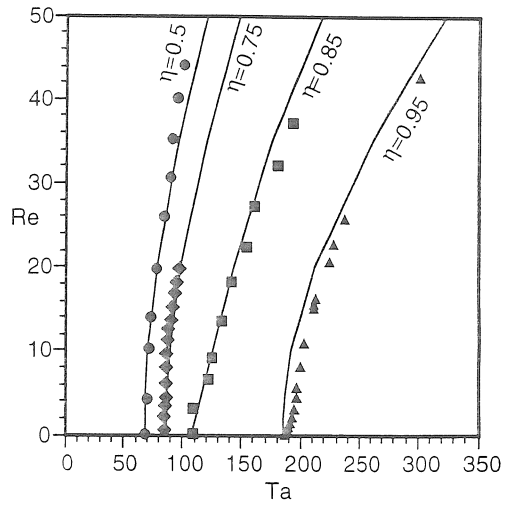

FIG. 6. Comparison of the transition boundary for the primary instability from Couette–Poiseuille flow to vortex flow. Solid lines are based on Ref. 6. Symbols indicate experimental results: ●, Takeuchi and Jankowski[7] (η=0.5, Γ=51); ◆, Babcock *et al.*[14] (η=0.738, Γ=144); ▲, Snyder[9] (η=0.952, Γ=260); ■, present study (η=0.848, Γ=41).

of reflected light. These helical vortices form nearly square cells with an axial wavelength of 1.8d. Like the nonwavy helical vortices (HV), the helix angle is 2.7°.

An unusual flow was found in a very small region of the Ta-Re plane that consists of a stationary helical vortices, denoted SHV in Fig. 4, and shown in Fig. 7(c). The axial wavelength of the stationary helical vortices is 1.7d. Unlike other helical vortices, the vortices in this flow regime do not move in the axial or azimuthal direction, but appear stationary. Surprisingly, the stationary helical vortices have a positive helix angle of 4.5° with respect to the direction of flow. This contradicts previous analytical and experimental results, which indicate that the vortices have a helix angle of opposite sign to that of the basic flow.[6,8,30] However, Takeuchi and Jankowski[7] suggest that there is no theoretical basis upon which to select the sign of the helical vortex angle, even though their analysis was restricted to helix angles opposite that of the basic flow. Based on an approximation of the average azimuthal velocity, $r_i\Omega/2$, and axial velocity, w, the inclination of the fluid path for the flow shown in Fig. 6(c) is about 3.8°. The similarity between the helix angle and the inclination of basic flow suggests that the basic fluid path may act to prescribe the helix angle of the stationary helical vortices. However, this flow only occurs over a narrow range of Reynolds and Taylor numbers, even though many other combinations of Reynolds and Taylor numbers that would result in the same fluid path inclination are possible. As indicated in Fig. 4, this flow regime is surrounded by the WV regime, but it is very close to the LV and HWV regimes. Bühler and Polifke[22] found a stationary helical vortex regime at similar Re and Ta, but the inclination of the vortices was opposite that of the flow. The reason for the difference between their results and the present study is unclear.

A large region of the stability map bounded by helical

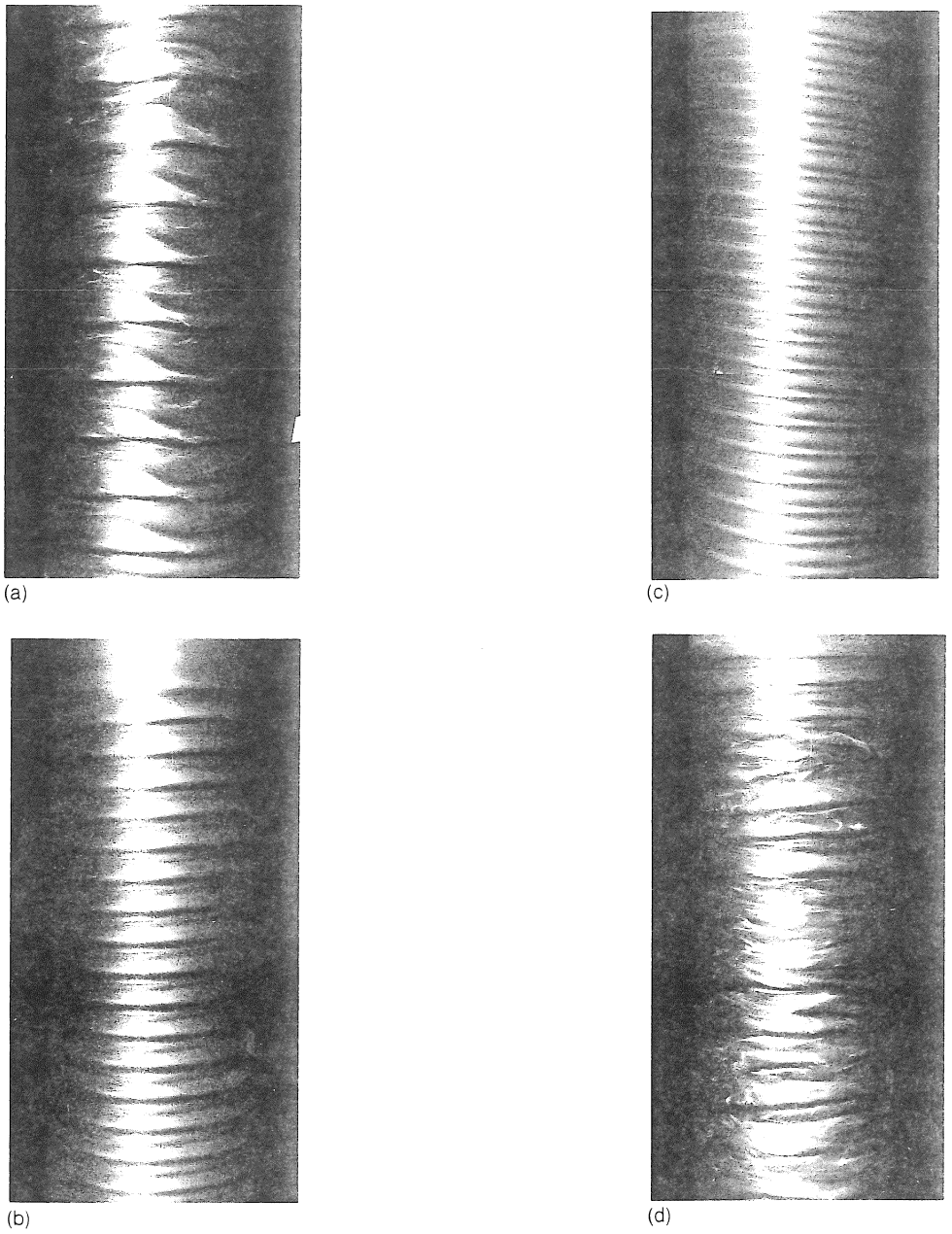

FIG. 7. (a) Flow visualization of wavy vortices (WV) for Re$\approx$3 and Ta$\approx$500. (b) Flow visualization of helical wavy vortices (HWV) for Re$\approx$10 and Ta$\approx$150. (c) Flow visualization of stationary helical vortices (SHV) for Re$\approx$5 and Ta$\approx$150. (d) Flow visualization of random wavy vortices (RWV) for Re$\approx$40 and Ta$\approx$600.

wavy vortices (HWV) at low Taylor numbers and toroidal wavy vortices (WV) at a higher Taylor number consists of a flow regime with a poorly defined wavy structure. This random wavy vortex flow (RWV) consists of wavy vortices that change shape rapidly, often with dislocations in the structure appearing, as shown in Fig. 7(d). Because of the random structure, the power spectrum of this flow contained no peaks, only an elevated amplitude at lower frequencies. The appearance of peaks above this noise level was used to differentiate this flow from HWV and WV. However, no sharp boundary between HWV and RWV or between RWV and WV could be identified. In fact, RWV may be considered to be a broad transition boundary between HWV and WV. Both a helical structure and a toroidal structure can be seen in the flow visualization at different instants, but no distinction was made between the two because of the randomness with which they appeared and disappeared. The helical structure was more likely to occur at low Taylor numbers, adjacent to the HWV regime. The wavy structure was more likely to occur at higher Taylor numbers, adjacent to the WV regime.

At zero axial Reynolds numbers, a flow regime of modulated wavy vortices (MWV) appeared for Taylor numbers between about 950 and 1350, as shown in Fig. 3. At slightly higher Reynolds numbers and Taylor numbers the vortices became turbulent, although the modulated waviness was retained (TMW), as shown in Fig. 8(a). The modulation of the waviness, sometimes seen as a subtle

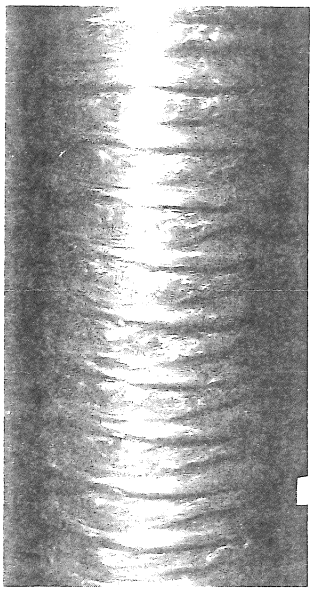

(a)

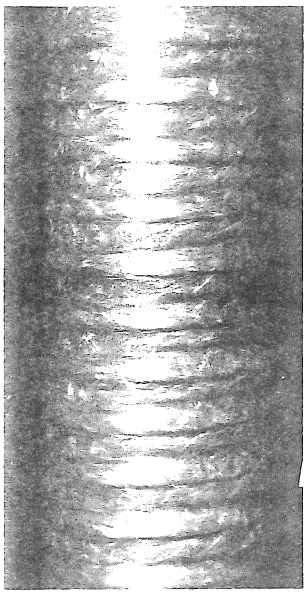

(b)

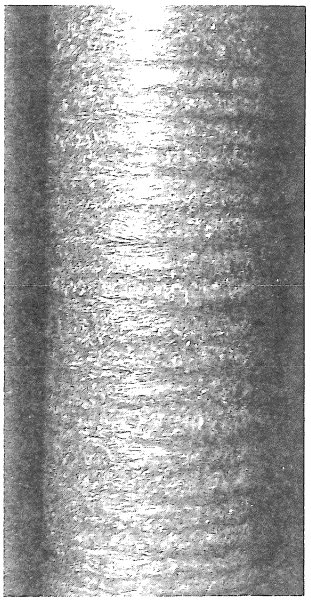

(c)

FIG. 8. (a) Flow visualization of turbulent modulated wavy vortices (TMW) for Re≈3 and Ta≈1100. (b) Flow visualization of turbulent wavy vortices (TWV) for Re≈3 and Ta≈1000. (c) Flow visualization of turbulent vortices (TV) for Re≈10 and Ta≈2500.

flattening of some of the waves, is probably hidden by the turbulent fluctuations. However, a spectral peak associated with the modulation appeared in the power spectrum of the reflected laser light. The axial wavelength of the vortices in Fig. 8(a) is $3.2d$.

The amplitude of the spectral peak associated with the modulation decreases as the Reynolds number is increased until turbulent wavy vortices (TWV), shown in Fig. 8(b), result. The turbulence makes the waviness difficult to observe directly, although a spectral peak related to the waviness appears in the power spectrum of the reflected light. When the Reynolds number exceeds 6, the modulated wavy vortex flow does not appear at all and wavy vortex flow (WV) transitions only to turbulent wavy vortex flow (TWV) with increasing Taylor number. The axial wavelength of the vortices in Fig. 8(b) is $3.0d$.

At very high Taylor numbers a regime of turbulent Taylor vortices (TV) that translate downstream with the axial flow was found. Consistent with the structure of these vortices when no axial flow is present,[19,31] the large-scale structure of toroidal vortices is retained. The turbulence is evident in the small-scale structure of the flow, as shown in Fig. 8(c). Here the axial wavelength is $3.3d$. It is evident from Fig. 3 that the axial flow destabilizes the Couette flow for low Reynolds numbers, resulting in transition to turbulent Taylor vortices at a lower Taylor number. However, larger Reynolds numbers do not seem to further destabilize the flow, as is evident in the location of the boundary between TWV and TV flow regimes in Fig. 3.

At Reynolds numbers greater than 15 a transitional (TRA) flow regime appears in Fig. 3 between TWV and TV in which turbulent Taylor vortices, turbulent wavy vortices, and turbulent helical vortex flow appear sequentially. The sequence begins with the annulus filled with toroidal turbulent Taylor vortices. After 5–20 sec the flow distorts along the entire length of the annulus and the vortices become wavy, although they remain turbulent and toroidal. Once the waviness is established, a turbulent helical vortex is created at the upstream end of the annulus. Like the stationary helical vortex (SHV) flow, the turbu-

lent helical vortices have a positive helix angle. However, the turbulent helical vortex appears to move downstream, unlike the stationary helical vortex, displacing the turbulent wavy vortices. Before the entire annulus develops into helical flow, new toroidal turbulent Taylor vortices appear at the upstream end of the annulus and move downstream. All three flow regimes can exist simultaneously at different points along the length of the annulus. The intermittent appearance of this turbulent helical vortex flow in the transitional flow regime suggests that a turbulent helical vortex flow regime may exist by itself. Subsequent experiments indicate that a flow regime consisting of turbulent helical vortices occurs at Reynolds number about 60 and Taylor number about 2500, although the flow was not investigated in detail.

The flow regime map shown in Figs. 3 and 4 is somewhat different from that of previous researchers. Kataoka *et al.*[21] indicate a gradual transition from laminar vortex flow to turbulent vortex flow. They also only indicate a small region of wavy vortex flow (WV) compared to the results of the present work. However, direct comparison of the results of Kataoka *et al.* with the present results is difficult, because the radius ratio in their experiments, $\eta = 0.62$, was significantly smaller. In addition, the electrochemical technique used in their experiments was probably not very sensitive in identifying transitions from one flow regime to another. Likewise, Bühler and Polifke[22] offer a stability map for low Taylor numbers that has some similarity to our results with regard to the appearance of helical vortex flow regimes. However, their results lack sufficient detail about the transition boundaries between flow regimes for direct comparison.

Although this study was not intended to measure the drift velocity of the vortices as they translate axially in the annulus, we note that the typical drift velocity for toroidal vortices calculated from the frequency of passage and vortex wavelength measured from the photos was 1.0–1.4 times the bulk axial velocity, regardless of the flow regime. The typical drift velocity for helical vortex flow was 1.5–1.8 times the bulk axial velocity, except for stationary spiral flow, where the vortices did not translate. The higher drift velocity for helical flow is a consequence of the combination of the downstream translation of the vortices and the apparent translation of vortices due to rotation of the helix, or the barber-pole effect.

The integral number of azimuthal waves for wavy vortex flows, m, was determined from the reflected light spectra using the relation $m \approx 0.34\Omega/f_1$, where Ω is the rate of rotation of the inner cylinder and f_1 is the azimuthal waviness frequency.[27,32] This result was checked visually by counting azimuthal waves for several cases. A map of the number of azimuthal waves is shown in Fig. 9. The number of azimuthal waves decreases with increasing Taylor number as it does with no axial flow.[32]

IV. SUMMARY

While previous studies of the stability of circular Couette flow with an imposed axial flow have been concerned with the primary transition of the flow from stable

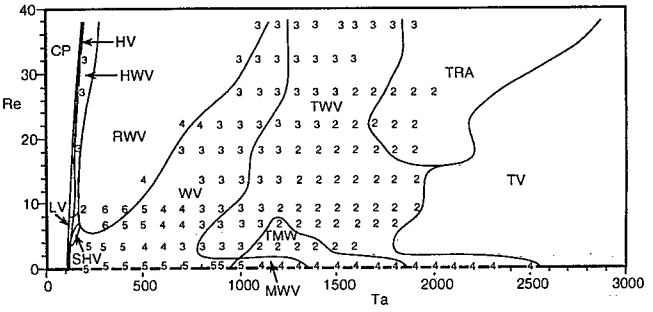

FIG. 9. Number of azimuthal waves for wavy flow regimes at each measurement point.

Couette–Poiseuille flow to Taylor vortex flow, we have considered higher-order transitions. Figures 3 and 4 are the central result of this research. While these figures provide a map of stability in the Re-Ta plane, this map is only valid for the radius ratio, $\eta = 0.85$, studied here. Other radius ratios should have qualitatively similar results, although the quantitative results may be different. Use of the Taylor number in a form including the radius ratio such as $T = \mathrm{Ta}^2[4(1-\eta)/(1+\eta)]$ may permit rough comparisons between these results and those at other radius ratios.

Several flow regimes that appear are similar to those that exist for no axial flow, except that the toroidal vortices are carried downstream with the axial flow. Helical vortex flow appears at higher Reynolds numbers to replace toroidal vortices. At low Taylor numbers both nonwavy and wavy helical flows appear. In addition, a unique stationary helical vortex (SHV) flow results that has a helix angle opposite that of all other helical flows. At high Taylor number and Reynolds numbers a turbulent helical vortex flow was found, although this flow was not investigated in detail. Two additional flow regimes (RWV and TRA) were found that appear to be less-ordered combinations of flow regimes bounding them. Further investigation of flows at higher Reynolds numbers than used in this study are necessary to complete the stability map for circular Couette flow with an imposed axial flow.

ACKNOWLEDGMENTS

A.D. was supported by the Deutscher Akademischer Austauschdienst. This work was supported by grants from Baxter Healthcare and the Whitaker Foundation.

[1] S. Chandrasekhar, "The hydrodynamic stability of viscid flow between coaxial cylinders," Proc. Natl. Acad. Sci. **46**, 141 (1960).

[2] R. C. DiPrima, "The stability of a viscous fluid between rotating cylinders with an axial flow," J. Fluid Mech. **9**, 621 (1960).

[3] M. A. Hasoon and B. W. Martin, "The stability of viscous axial flow in an annulus with a rotating inner cylinder," Proc. R. Soc. London Ser. A **352**, 351 (1977).

[4] R. C. DiPrima and A. Pridor, "The stability of viscous flow between rotating concentric cylinders with an axial flow," Proc. R. Soc. London Ser. A **366**, 555 (1979).

[5] In this paper we avoid the term "spiral," which has been used in two ways in previous studies of this flow. First, the term "spiral flow" has been used to identify the spiral path of a fluid particle associated combined stable laminar circular Couette flow and stable laminar pressure-driven axial flow. Second, the term "spiral vortices" has been used to

describe an instability that appears as a helical vortex structure.
[6]K. C. Chung and K. N. Astill, "Hydrodynamic instability of viscous flow between rotating coaxial cylinders with fully developed axial flow," J. Fluid Mech. **81**, 641 (1977).
[7]D. I. Takeuchi and D. F. Jankowski, "A numerical and experimental investigation of the stability of spiral Poiseuille flow," J. Fluid Mech. **102**, 101 (1981).
[8]B. S. Ng and E. R. Turner, "On the linear stability of spiral flow between rotating cylinders," Proc. R. Soc. London Ser. A **382**, 83 (1982).
[9]H. A. Snyder, "Experiments on the stability of spiral flow at low axial Reynolds numbers," Proc. R. Soc. London Ser. A **265**, 198 (1962).
[10]K. W. Schwarz, B. E. Springett, and R. J. Donnelly, "Modes of instability in spiral flow between rotating cylinders," J. Fluid Mech. **20**, 281 (1964).
[11]R. J. Donnelly and D. Fultz, "Experiments on the stability of spiral flow between rotating cylinders," Proc. Natl. Acad. Sci. **46**, 1150 (1960).
[12]N. Gravas and B. W. Martin, "Instability of viscous axial flow in annuli having a rotating inner cylinder," J. Fluid Mech. **86**, 385 (1978).
[13]M. M. Sorour and J. E. R. Coney, "The characteristics of spiral vortex flow at high Taylor numbers," J. Mech. Eng. Sci. **21**, 65 (1979).
[14]K. L. Babcock, G. Ahlers, and D. S. Cannell, "Noise-sustained structure in Taylor–Couette flow with through flow," Phys. Rev. Lett. **67**, 3388 (1991).
[15]A. Tsameret and V. Steinberg, "Noise-modulated propagating pattern in a convectively unstable system," Phys. Rev. Lett. **67**, 3392 (1991).
[16]J. Kaye and E. C. Elgar, "Modes of adiabatic and diabatic fluid flow in an annulus with an inner rotating cylinder," Trans. Am. Soc. Mech. Eng. **80**, 753 (1958).
[17]K. M. Becker and J. Kaye, "Measurements of diabatic flow in an annulus with an inner rotating cylinder," J. Heat Transfer **84**, 97 (1962).
[18]K. Beranek, I. Streda, and J. Sestak, "On the flow of viscous liquids through annular clearances with the rotating inner cylinder," Acta Technol. CSAV **24**, 65 (1979).
[19]P. R. Fenstermacher, H. L. Swinney, and J. P. Gollub, "Dynamical instabilities and the transition to chaotic Taylor vortex flow," J. Fluid Mech. **94**, 103 (1979).
[20]C. D. Andereck, S. S. Lui, and H. L. Swinney, "Flow regimes in a circular Couette system with independently rotating cylinders," J. Fluid Mech. **164**, 155 (1986).
[21]K. Kataoka, H. Doi, and T. Komai, "Heat/mass transfer in Taylor vortex flow with constant axial flow rates," Int. J. Heat Mass Transfer **20**, 57 (1977).
[22]K. Bühler and N. Polifke, "Dynamical behaviour of Taylor vortices with superimposed axial flow," in *Nonlinear Evolution of Spatio-Temporal Structures in Dissipative Continuous Systems*, edited by F. H. Busse and L. Kramer (Plenum, New York, 1990).
[23]O. Savas, "On flow visualization using reflective flakes," J. Fluid Mech. **152**, 235 (1985).
[24]M. A. Dominguez-Lerma, G. Ahlers, and D. S. Cannell, "Effects of 'Kalliroscope' flow visualization particles on rotating Couette–Taylor flow," Phys. Fluids **28**, 1204 (1985).
[25]E. M. Sparrow, W. D. Munro, and V. K. Jonsson, "Instability of the flow between rotating cylinders: The wide gap problem," J. Fluid Mech. **20**, 35 (1964).
[26]P. H. Roberts, "The solution of the characteristic value problem," Proc. R. Soc. London Ser. A **283**, 550 (1965).
[27]M. Gorman and H. L. Swinney, "Spatial and temporal characteristics of modulated waves in the circular Couette system," J. Fluid Mech. **117**, 123 (1982).
[28]R. C. DiPrima and H. L. Swinney, "Instabilities and transition in flow between concentric rotating cylinders," in *Topics in Applied Physics, Hydrodynamic Instabilities and the Transition to Turbulence*, edited by H. L. Swinney and J. P. Gollub (Springer-Verlag, Berlin, 1985).
[29]M. G. Short and J. H. Jackson, "Wavy mode superlaminar flow between concentric and eccentric rotating cylinders: Stroboscopic flow visualization and torque measurement," in 2nd *Leeds–Lyon Symposium on Tribology*, 16–19 September 1975 (Burlington, London, 1975).
[30]H. A. Snyder, "Experiments on the stability of two types of spiral flow," Ann. Phys. **31**, 292 (1965).
[31]J. E. Burkhalter and E. L. Koschmieder, "Steady supercritical Taylor vortex flow," J. Fluid Mech. **58**, 547 (1973).
[32]D. Coles, "Transition in circular Couette flow," J. Fluid Mech. **21**, 385 (1965).

V23.

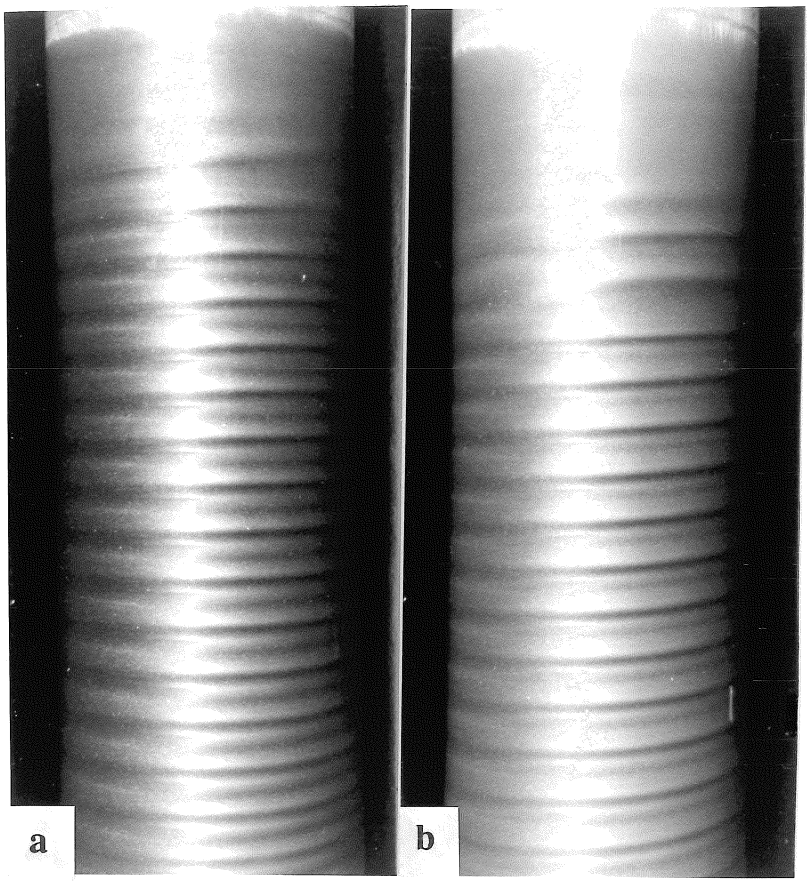

Fig. 4 5
Lueptow and Docter
single column figure
planned for 4:3 reduction

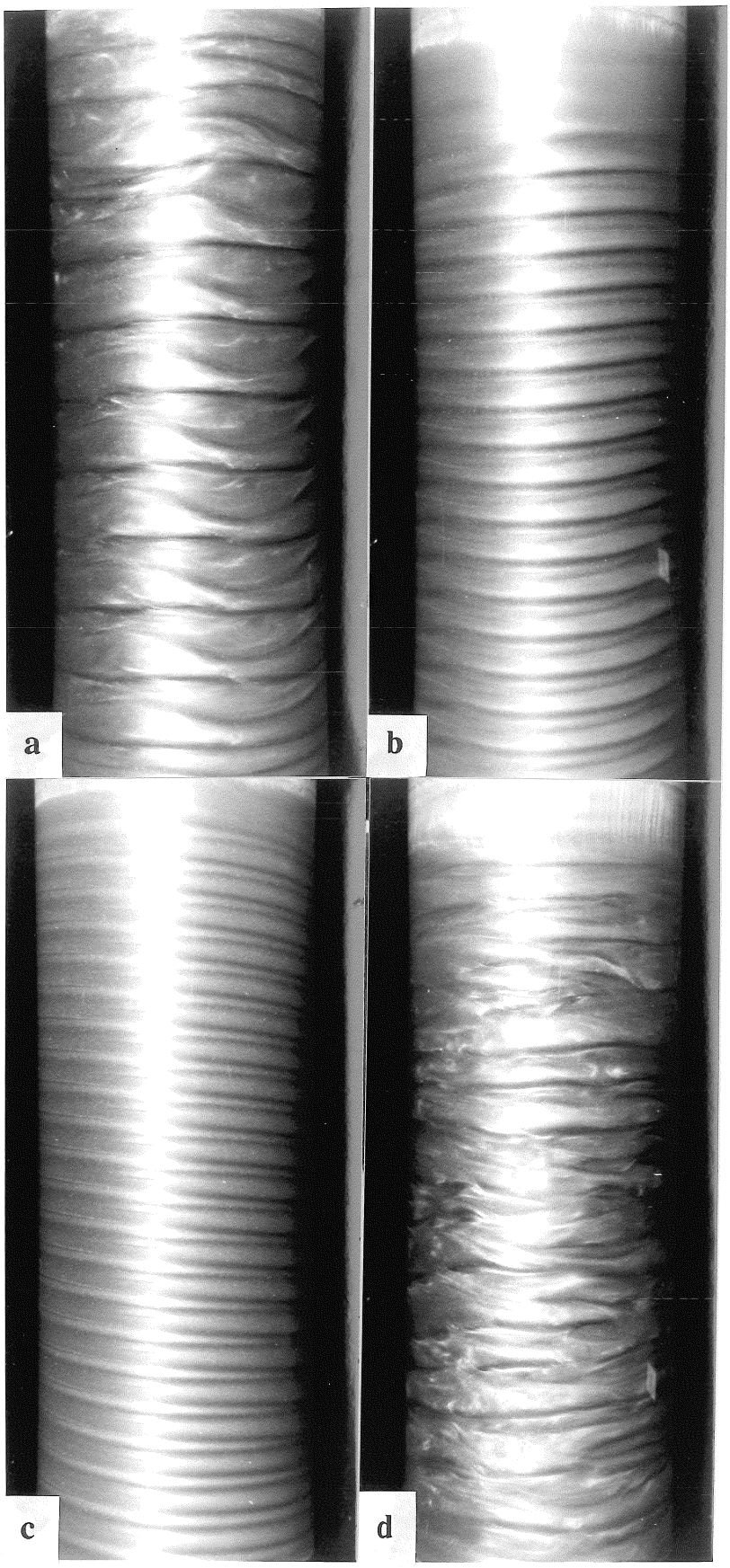

Fig. 7
Lueptow and Docter
single column figure
planned for 4:3 reduction

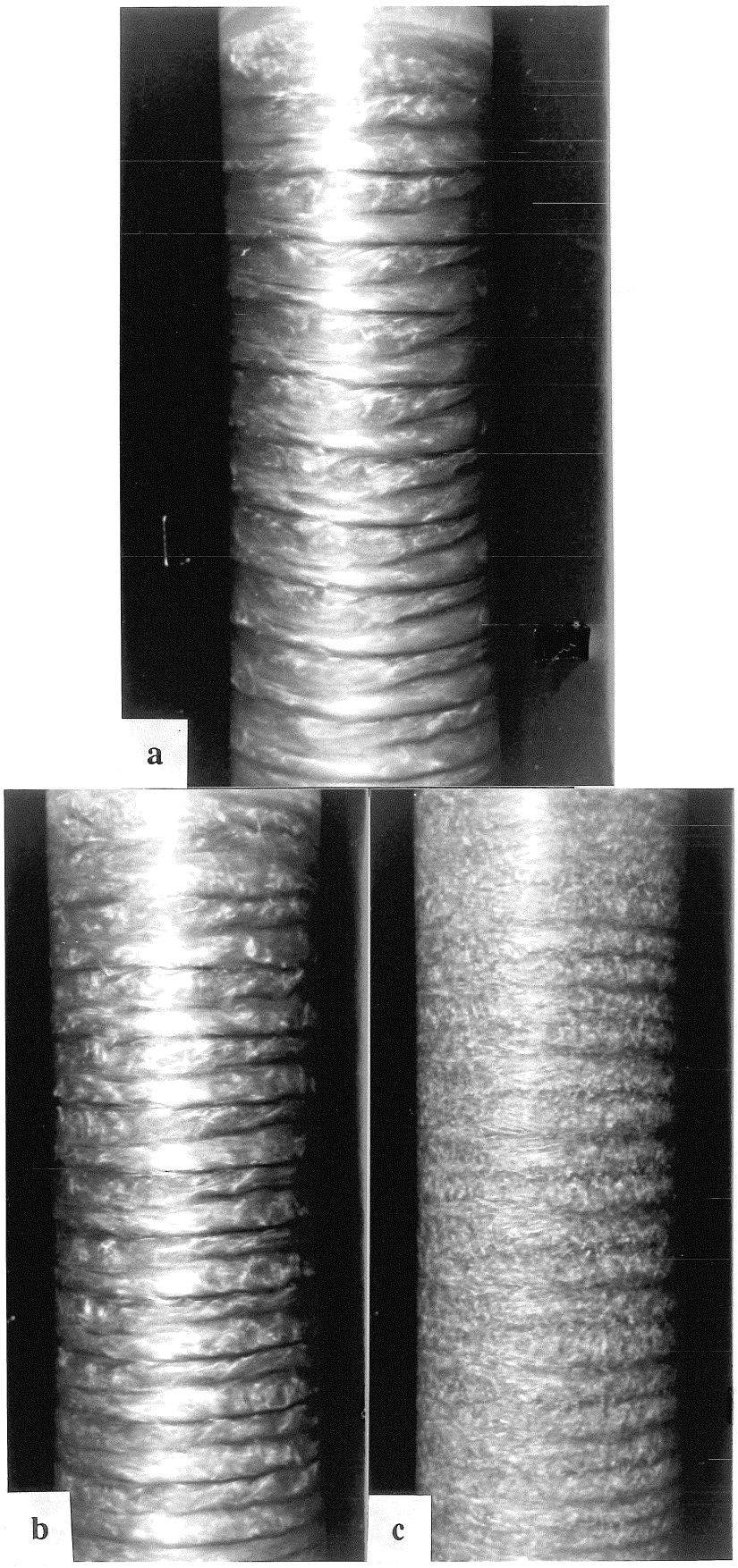

Fig. #3
Lueptow and Docter
single column figure
planned for 4:3 reduction